Journal of Materials Chemistry C

COMMUNICATION

Polymeric Mold Soft-Patterned Metal Oxide Field-Effect Transistors: Critical Factors Determining Device Performance

Seong Jip Kim,[a,b,§] Aryeon Kim,[a,§] Yejin Jo,[a] Jun-Young Yoon,[a] Sun Sook Lee,[a] Youngmin Choi,[a] Jong Chan Won,[a] Sahn Nahm,[b] Kwang-Suk Jang,[a,*] Yun Ho Kim,[a,*] Sunho Jeong[a,*]
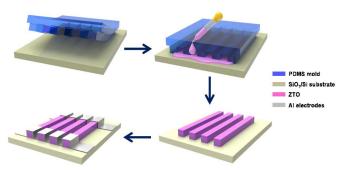
During the last decade, metal oxide semiconductors have received significant attention as promising channel materials for implementation in thin-film transistors (TFTs) as alternatives to conventional Si semiconductors. They have been demonstrated capable of being mass produced in large area and to provide improved device performances.[1,2] In particular, the soluble metal oxide semiconductors have been widely researched due to their characteristic advantages, including low-cost scalable deposition and device performance comparable to vacuum-deposited counterparts.[3] Recent active researches on new chemical approaches and unconventional post-treatment methodologies have now resolved the issues of low temperature processability, making them compatible even with plastic substrates, and high field-effect mobilities over 10 $cm^2/V \cdot s$ have been reported for devices with spin-cast, non-patterned channel layers.[4-7] Significant effort has been invested in improving the inherent properties of soluble metal oxide semiconductors. However, polymeric mold based roll-to-roll (R2R) patterning techniques, which are essential for defining device architectures with high throughput, have not been successfully demonstrated. R2R printing technologies offer significant advantages for the use of soluble oxide semiconductors, and provide a superior alternative to vacuum deposited metal oxides, whose fabrication typically involves a time consuming, complicated photolithography technique.

Organic semiconductors are another viable type of soluble semiconductor for TFTs, and have been demonstrated with various printing methodologies, including a jet printing,[8] a screen printing,[9] R2R printings of a gravure printing[10] and a flexographic printing[9]. Furthermore, the controllable ability to spatially arrange organic semiconductors inside wet films has facilitated evaporation-induced device performance modulation[11,12] and a simple bar coating process over an extremely large area.[13] In contrast to these techniques, the fabrication of patterned structures of inorganic metal oxide semiconductors has mainly been proposed using jet printing techniques.[7,13-16] Electric field assisted jet printing devices have shown fine resolution processability when defining the channel geometry.[15,16] However, jet based printing methods possess drawbacks which limit practical mass production, as compared with polymeric mold based R2R techniques. In large-area applications, the jet printing technique often suffers from limited ability to reproducibly control the individual jetting behavior in nozzles, which may number as many as 100 or more, and this restricts the production yield and the uniformity of device performance. In the case of polymeric mold based R2R printing techniques, the uniformity and the production yield over a large area are determined mainly by the preparation accuracy of the polymeric mold and/or the patterned substrate, a so-called cliché, which can be resolved with well-developed mechanical processing methods. Notably, other than jet printed devices, the chemical imprinting method, which involves the selective dissolution of preformed metal oxide films,[17] and the spray pyrolysis method have successfully demonstrated device-quality patterned structures.[18] Interestingly, these methods are not associated with solvent evaporation in confined structures. For jet printing methodologies, the micro-droplets ejected through nozzles undergo significantly accelerated solvent evaporation during their trajectory toward a substrate, and thus accumulate as a semi-solid phase, forming the patterned structures. The polymeric mold based printing techniques involve the adjustment of solvent evaporation in liquid-like wet films to facilitate the sequential transfer between the mold and a substrate. To date, a soluble In-Ga-Zn-O (IGZO) device produced by a gravure printing method has been reported to have a field-effect mobility below 1 $cm^2/V \cdot s$, after annealing at 550 °C[19] and high performance gravure printed devices with a field-effect mobility above 10 $cm^2/V \cdot s$ have been demonstrated after transferring the sputtered IGZO films.[20]

Herein, we study the critical determining factors in device performance of TFTs employing metal oxide channels formed by mold based soft-patterning processes involving solvent evaporation. For a model patterning procedure, we choose the micro molding in capillary (MIMIC) method to independently investigate the properties of oxide patterns formed with solvent evaporation in mold structures, excluding the factors associated with transferring procedures in roll-to-roll processes. Among various compositional candidates for metal oxide semiconductors, zinc tin oxide (ZTO) is selected for the study, owing to its material issues, earth abundance of elemental components, moderate field-effect mobility, and the difficulty in defining patterned ZTO structures by a wet etching. In

addition, in order to investigate how the different chemical approaches to synthesizing the soluble precursor solutions affect the variation of chemical/electrical properties, three representative types of precursor solutions are prepared. Through spectroscopic analysis on chemical structural evolutions and a comparative analysis of the device performances for both MIMIC patterned and spin-cast ZTO TFTs, the constraining factors that limit the device performance of TFTs employing soft-patterned oxide semiconductors are elucidated.

The ZTO sol-gel precursor solutions were prepared in three different ways by synthesizing the conventional metal salt (MS) derived, the combustion chemistry (CC) involved, and chemical additive (CA) mediated ZTO semiconductors, which are denoted as MS-ZTO, CC-ZTO, and CA-ZTO, respectively. In combustion chemistries, the exothermic reaction induced by the molecular combination of a fuel and an oxidizer facilitates the high performance oxide TFTs by providing an additional internal thermal energy.[7,21] In the case of chemical additive approaches, the properly incorporated additive, either ethylene glycol or formamide, acts as a catalyst for sol-gel reactions and allows for the formation of an oxide skeleton framework more suitable for high performance TFTs.[3,16,22] Other than metal salt-based sol-gel chemistries, the methodologies for preparing precursor solutions suffer from the limited availability of precursor materials, and the nanoparticle based approaches have not shown acceptable high device performance, owing to the inefficient charge transport between neighboring nanoparticles.[23]

For a comparative study of both the widely tested spin-cast, and MIMIC soft-patterned ZTO channel layer, both types of ZTO films were fabricated. The MIMIC patterned ZTO structures were prepared following a conventional soft-patterning technique (Scheme 1), similar to the previous report for ITO nanoparticle-based TFTs.[24] The patterned PDMS mold was placed on a SiO_2/Si substrate to generate micro channels, which were filled by applying ZTO precursor solutions at one end. Then, the solution was infiltrated into the channels by capillary force, and the PDMS mold was removed to leave ZTO stripe patterns on the substrates after evaporating the solvent, 2-methoxyethanol, at 60 °C for 5 min. The MS-ZTO and the CA-ZTO layers were annealed at 400 °C for 2 hr

Scheme 1. A pre-patterned PDMS mold was placed on the top of a SiO_2/n$^+$-Si substrate, and the prepared ZTO precursor solutions were poured gently at the side of the micro-channels. After completely drying the solvent at 60 °C, the PDMS mold was gently removed, followed by a thermal annealing at a specific temperature, either 350 or 400 °C. The Al electrodes were deposited by a thermal evaporation on the resulting patterned oxide structures for complete device architectures.
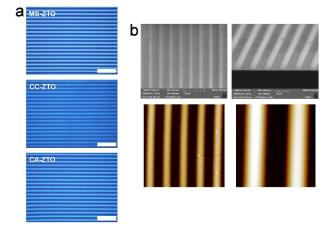
Figure 1. (a) Optical microscopy images of MIMIC soft-patterned MS-ZTO, CC-ZTO, and CA-ZTO layers. The scale bar is 50 μm. (b) Scanning microscopy images and atomic force microscopy images for MIMIC soft-patterned MS-ZTO layers. The measurement areas for the left and right AFM image were 50×50, and 20×20 μm^2, respectively.

in air, and the CC-ZTO layer was annealed at 350 °C for 2 hr in air. Figure 1a shows the optical microscopy images of the MIMIC soft-patterned ZTO structures. It was observed that well patterned, fine structures were generated in all of the observation area, regardless of the kind of precursor solution. The width and height of patterns in the PDMS mold tested in this study were 5 and 1 μm, respectively. The linewidth of ZTO patterns was measured to be ~5 μm, which corresponds to the width of the PDMS mold patterns. This implies that the volumetric contraction resulting from successive solvent evaporation proceeds along a sidewall of the PDMS mold, which introduces a capability for controlling the linewidth. The uniformly patterned structures were also observable in scanning electron microscopy images, and the surface smoothness along the surface of the ZTO patterns was confirmed with atomic force microscopic images (Figure 1b).

Figure 2 shows the O 1s X-ray photoelectron spectroscopy (XPS) spectra and the semi-quantitative analysis obtained from the individual areal integration of sub-peaks, for both spin-cast and MIMIC soft-patterned ZTO films. For all of the spin-cast MS-, CC-, and CA-ZTO films, the peaks located around 530.3 and 531.9 eV are attributed to the oxide lattice without oxygen vacancies (O_o^x) and with oxygen vacancies ($V_o^{\cdot\cdot}$), respectively.[25,26] The peak at 532.5 eV originated from the hydroxyl group. Similarly, for MIMIC patterned ZTO films, O_o^x and $V_o^{\cdot\cdot}$ were detected at 530.3 and 531.9 eV, respectively. However, interestingly, the peak due to the hydroxyl group shifted toward a higher binding energy, up to 532.7, 533.3, and 533.0 eV for soft-patterned MS-, CC-, CA-ZTO films, respectively, and unknown peaks appeared at binding energies over 534 eV. According to the semi-quantitative analysis, it was revealed that when all of the ZTO layers were formed through a MIMIC patterning process, the fraction of oxide lattice, $O_o^x + V_o^{\cdot\cdot}$, was noticeably reduced, and the fraction of hydroxyl groups increased. This chemical structural evolution toward a metal oxide framework composed of more hydroxides, along with the presence of peaks at high binding energies, is one of the characteristic features observed for incomplete sol-gel reaction involved metal oxide films.[27] In metal salt sol-gel chemistries,
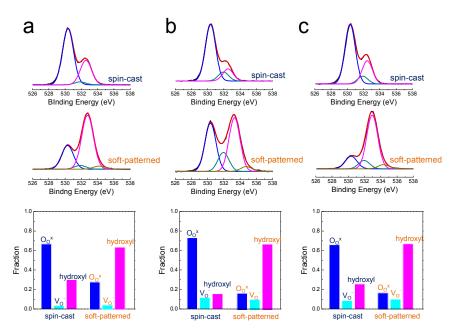
Figure 2. O 1s spectra and semi-quantitative results of each sub-peak in O1s spectra for both spin-cast and MIMIC soft-patterned ZTO layers derived from (a) MS-ZTO, (b) CC-ZTO, and (c) CA-ZTO precursor solutions. All ZTO films were annealed on preheated hotplates.

the chemical form of precursors can be varied depending on the preparation approaches. Unlike the conventional MS-ZTO, the anion that acts as either a fuel or an oxidizer is present for CC-ZTO, and the cations are reacted with chemical additives forming the complexes for CA-ZTO. However, the basic reaction scheme is identical for all of the approaches: stepwise, subsequent reactions of metal cations by a hydration, a hydrolysis, and a condensation. For this reason, it can be speculated that a similar suppressed trend in chemical structural evolutions was detected for MIMIC soft-patterned films, for all of the precursor solutions.

In principle, during the sol-gel reactions, metal cations are solvated with water molecules, and subsequently undergo a hydrolysis reaction through the loss of a proton from the water molecules surrounding the metal cation in the first solvation shell. As a consequence, the aquo ligand molecule, H_2O, is chemically converted into either a hydroxo ligand, OH^-, or into an oxo ligand, O^{2-},[28] and the condensation reaction takes place, evolving an oxo-bridge, M-O-M, enabling the formation of a metal oxide skeleton framework. Those subsequent reactions occur partially even at room temperature in air, which is confirmed by the fact that precipitates form in concentrated precursor solutions after a prolonged time at room temperature. When thermal energy is supplied by heating thin films derived from precursor solutions, the reactions are accelerated, resulting in chemical structures with oxide lattices, hydroxides by the incomplete condensation reaction, and impurities by the incomplete thermal decomposition, depending on annealing temperatures. However, in addition to the influence of thermodynamics, these sol-gel reactions are critically influenced by kinetics in supplying the thermal energy as a driving force for reactions; when the thermal energy is provided more instantly to the films, the chemical structures with more oxide lattices, which are favorable for high performance TFTs, are generated. As shown in Figure S1, all of the ZTO films annealed on the preheated hotplate at desirable temperatures (400 ^{o}C for MS-ZTO and CA-ZTO, and 350 ^{o}C for CC-ZTO)

exhibited much better device performances, compared with the identical devices employing ZTO channels annealed on the hotplate with a heating rate of 5 ^{o}C/min. This characteristic behavior is not limited to the case of ZTO TFTs. For soluble In-Ga-Zn-O (IGZO) devices, the discrepancy in device performances between the two annealing methods was also observed (Figure S2). All of the device parameters were summarized in Table S1.

In the case of a solvent evaporation involved MIMIC process, the micro channels between the substrate and a PDMS mold are filled with a precursor solution, and the structural formation into patterned solvent-free precursor films occurs while the solvent evaporates through the overall PMDS mold. As the solvent is gradually evaporated, the concentration of precursors in the structurally confined liquid channels increases; then, upon approaching a critical concentration, the sol gel reaction is accelerated, partially triggering the chemical structural evolution at a drying temperature of 60 ^{o}C. As shown in Figure S3, as the bulk precursor solution is being dried at 60 ^{o}C, the viscosity almost linearly increases due to the gradual evaporation of solvents, and abruptly goes out of linear behavior across a characteristic time-dependent drying zone; this indicates the evaporation induced initiation of sol-gel reactions at a moderate temperature of 60 ^{o}C, which is commonly observed in classical sol-gel chemistry reactions.[29] At drying temperatures above 60 ^{o}C, the uniformly patterned structures could not be reproducibly obtained because of the vigorous evaporation of the solvent, 2-methoxyethanol, whose boiling point is 128 ^{o}C. At room temperature, it took at least 4 hrs to dry the infiltrated precursor solutions since the solvent evaporation through the PDMS mold is inhibited. It is presumed that the gradually proceeding partial sol-gel reaction, induced in time-dependently concentrated solutions at moderately elevated temperatures, gives rise to chemical structures that are likely to undergo limited kinetics in supplying the driving force for reactions. This was the case with ZTO films annealed on a hot plate with a slow ramping
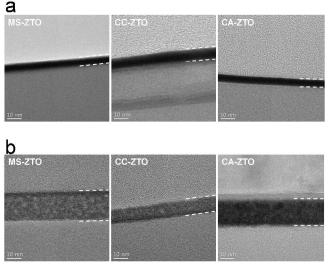
Figure 3. HRTEM Images for (a) the spin-cast and (b) MIMIC soft-patterned ZTO layers. All of ZTO films were annealed on preheated hotplates. The dashed lines indicate the boundaries of ZTO films located between upper epoxy layers and lower SiO_2 layers.

rate. In contrast, for the spin-cast films, the solvent-free precursor layers are obtained by instant solvent evaporation at room temperature, with the structural confinement into film morphologies resulting from intense centrifugal force for a time scale of seconds. This pristine precursor film, rather than experiencing the driving force of sol-gel reactions at room temperature for a very short time, is likely to be the case in jet printed semi-solid droplets, with a volume dimension of a few tens of picoliter, formed by accelerated evaporation during a trajectory.

The distinctively different film qualities were also confirmed with high resolution transmission electron microscopy (HR-TEM) images, as shown in Figure 3. The contrast in TEM images for thin films indicates the presence of nano-sized voids. It was clearly observed that the MIMIC soft-patterned ZTO films show more porous film structures compared with spin-cast ones, even though they were annealed at identical temperatures in the same way. In sol-gel chemistries accompanied by the formation of oxo-bridge chemical binding by the successive removal of by-products and impurities, less dense structural properties imply that the chemical reactions were incomplete, not forming the oxide films fully composed of oxide lattices without hydroxides and impurities.

Figure 4 shows both the transfer and output characteristics for TFTs employing MS-, CC-, CA-ZTO channel layers prepared by the spin-casting and MIMIC soft-patterning processes. The TFTs were fabricated with a device architecture of bottom gate/top contact, by forming the ZTO channel layers on 100 nm-thick SiO_2/n^+-Si substrates, followed by a thermal annealing and a thermal evaporation of Al source/drain electrodes. The representative device parameters were summarized in Table 1. The field-effect mobilities of TFTs with spin-cast MS-, CC-, CA-ZTO channel layers were measured to be 4.1, 7.4, and 7.6 $cm^2/V \cdot s$, respectively. This is in contrast to previously reported soluble ZTO TFTs, where the field-effect mobilities have been limited to values around 3 $cm^2/V \cdot s$ after annealing at temperatures below 400 ^oC.[30] The spin-cast ZTO devices tested in this study exhibited improved
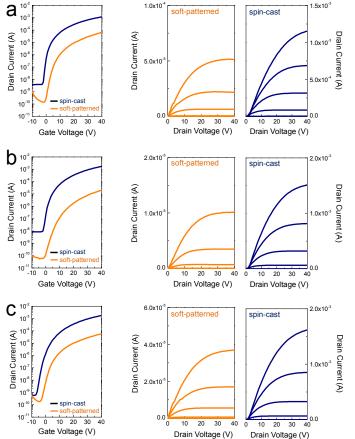

Figure 4. Transfer and output characteristics for TFTs employing the spin-cast and MIMIC soft-patterned ZTO channel layers derived from (a) MS-ZTO, (b) CC-ZTO, and (c) CA-ZTO precursor solutions. All ZTO films were annealed on preheated hotplates.

device performance with field-effect mobilities exceeding 7 $cm^2/V \cdot s$. This was achieved by introducing characteristic combustion chemistry and chemical additive approach into the ZTO material systems. To date, the use of both methodologies has been restricted to In-added materials, such as In_2O_3, In-Zn-O, and In-Ga-Zn-O, all of which incorporate indium as a mobility enhancer.[3,7,16,21,22] However, as expected from the spectroscopic and microscopic results, the device performances were drastically degraded for TFTs employing MIMIC soft-patterned ZTO channel layers, exhibiting field-effect mobilities of 0.9, 0.3, and 0.6 $cm^2/V \cdot s$ for MS-, CC-, and CA-ZTO channel layers, respectively. Even though they were prepared with identical procedures except for the film forming process, the ZTO devices prepared by the solvent evaporation involved MIMIC soft-patterning process showed lower field-effect mobilities by a factor of 4.6-15.7, with much lower drain currents in output characteristics, regardless of the types of precursor solutions. This implies that the device performance in soluble oxide TFTs is critically influenced by the method used in forming the solvent-free precursor films, and that it is even more important than the effect of sophisticatedly controlled synthetic pathways. Those results also suggest the meaningful fact that controlling the solvent evaporation-involved trigger of the sol-gel reactions is one of the most significant factors for

Table 1. Various ZTO channel layers were prepared either by a spin-casting or a MIMIC soft patterning method. MS-ZTO, CC-ZTO, and CA-ZTO represent the ZTO precursor solutions derived by a metal salt sol-gel chemistry, a combustion chemistry, and a chemical additive approach, respectively. All ZTO layers were annealed instantly on preheated hotplates

semiconductors		mobility (cn^2/Vs)	V_T (V)	$I_{on/off}$
MS-ZTO	spin-cast	4.1	-0.8	4×10^6
	soft-patterned	0.9	10.4	6×10^5
CC-ZTO	spin-cast	7.4	3.4	1×10^5
	soft-patterned	0.3	12.1	1×10^5
CA-ZTO	spin-cast	7.6	3.3	5×10^6
	soft-patterned	0.6	6.0	2×10^5

facilitating high performance devices when using polymeric mold-based soft-patterning processes, unlike the general spin-casting method and jet based printing techniques. It is expected that the additional input of other external forces for instant solvent evaporation, such as a high shearing force and a hot dry air, could be effective in forming solvent-free precursor films in a very short timescale, enough to sufficiently suppress the undesirable initiation of reactions, and thereby enabling the generation of high performance, soft-patterned soluble oxide TFTs in a high-throughput R2R process.

In summary, in order for exploring the factors limiting device performance in soluble oxide TFTs fabricated by polymeric mold-based patterning methodologies, we compared the chemical structures of either spin-cast or soft-patterned ZTO semiconductors and investigated the device performance of TFTs employing the two kinds of ZTO channel layers. Through the comparative analysis of both ZTO layers, it was revealed that less transformed chemical structures evolved in soft-patterned ZTO devices, with significantly degraded device performance, regardless of characteristic synthetic strategies. This variation in performance was caused by kinetics-involved, different chemical reaction pathways due to gradual solvent evaporation in structurally confined polymeric molds, which inevitably occurs in mold-based soft-patterning techniques. It is believed that this scientific finding, deduced from a comparative study using a model case study, may open a new possible path for exploiting high performance, soft-patterned oxide devices, including the use of high throughput mold-based R2R processes, by identifying the physical/chemical origin of the poor performance of devices reported to date.

Acknowledgements

Notes and references

[a] Division of Advanced Materials, Korea Research Institute of Chemical Technology (KRICT), Daejeon 305-600, Republic of Korea

E-mail: kjang@krict.re.kr (K.-S. Jang), yunho@krict.re.kr (Y.H. Kim), sjeong@krict.re.kr (S. Jeong)

[b] Department of Materials Science and Engineering, Korea University, Seoul, Republic of Korea

[§] These authors contributed equally to this work

1. K. Nomura, H. Ohta, K. Ueda, T. Kamiya, M. Hirano, H. Hosono, *Science* 2003, **300**, 1269.

2. L. Wang, M.-H. Yoon, G. Lu, A. Facchetti, T. J. Marks, *Nature Mater.* 2006, **5**, 893.

3. S. Jeong, J. Moon, *J. Mater. Chem.* 2012, **22**, 1243.

4. Y. -H. Kim, J.-S. Heo, T.-H. Kim, S. Park, M.-H. Yoon, J. Kim, M. S. Oh, G.-R. Yi, Y.-Y. Noh, S. K. Park, *Nature* 2012, **489**, 128.

5. K. K. Banger, Y. Yamashita, K. Mori, R. L. Peterson, T. Leedham, J. Rickard and H. Sirringhaus, *Nature Mater.* 2011, **10**, 45.

6. S.-Y. Han, G. S. Herman, C.-H. Chang, *J. Am. Chem. Soc.* 2011, **133**, 5166.

7. M.-G. Kim, M. G. Kanatzidis, A. Facchetti, T. J. Marks, *Nature Mater.* 2011, **10**, 382.

8. J. A. Lim, W. H. Lee, D. Kwak, K. Cho, *Langmuir* 2009, **25**, 5404.

9. M. M. Voigt, A. Guite, D. –Y. Chung, R. U. A. Khan, A. J. Campbell, D. D. C. Bradley, F. Meng, J. H. G. Steinke, S. Tierney, L. McCulloch, H. Penxten, L. Lutsen, O. Douheret, J. Manca, U. Brokmann, K. Sönnichsen, D. Hülsenberg, W. Bock, C. Barron, N. Blanckaert, S. Springer, J. Grupp, A. Mosley, *Adv. Funct. Mater.* 2010, **20**, 239.

10. B. Kang, W. H. Lee, K. Cho, *ACS Appl. Mater. Interfaces* 2013, **5**, 2302.

11. S. Liu, W. M. Wang, A. L. Briseno, S. C. B. Mannsfeld, Z. Bao, *Adv. Mater.* 2009, **21**, 1217.

12. J. A. Lim, W. H. Lee, H. S. Lee, J. H. Lee, Y. D. Park, K. Cho, *Adv. Mater.* 2008, **18**, 229.

13. D. Khim, H. Han, K.-J. Baeg, J. Kim, S.-W. Kwak, D.-Y. Kim, Y.-Y. Noh, *Adv. Mater.* 2013, **25**, 4302.

14. S. Dasgupta, R. Kruk, N. Mechau, H. Hahn, *ACS Nano* 2011, **5**, 9628.

15. S. Lee, J. Kim, J. Choi, H. Park, J. Ha, Y. Kim, J. A. Rogers, U. Paik, *Appl. Phys. Lett.* 2012, **100**, 102108,.

16. S. Jeong, J.-Y. Lee, S. S. Lee, Y.-H. Seo, S.-Y. Kim, J.-U. Park, B.-H. Ryu, W. Yang, J. Moon, Y. Choi, *J. Mater. Chem. C* 2013, **1**, 4236.

17. K. Seong, K. Kim, S. Y. Park, Y. S. Kim, *Chem. Comm.* 2013, **49**, 2783.

18. H. Faber, B. Butz, C. Dieker, E. Spiecker, M. Halik, *Adv. Funct. Mater.* 2013, **23**, 2828.

19. Y. Choi, G. H. Kim, W. H. Jeong, H. J. Kim, B. D. Chin, J.-W. Yu, *Thin Solid Films*, 2010, **518**, 6249.

20. B. K. Sharma, B. Jang, J. E. Lee, S.-H. Bae, T. W. Kim, H.-J. Lee, J.-H. Kim, J.-H. Ahn, *Adv. Funct. Mater.* 2013, **23**, 2024.

21. Y. H. Kang, S. Jeong, J. M. Ko, Ji. –Y. Lee, Y. Choi, C. Lee, S. Y. Cho, *J. Mater. Chem. C* 2014, **2**, 4247.

22. S. Jeong, J.-Y. Lee, S. S. Lee, S.-W. Oh, H. H. Lee, Y.-H. Seo, B.-H. Ryu, Y. Choi, *J. Mater. Chem.* 2011, **21**, 17066.

23. H. Faber, M. Burkhardt, A. Jedaa, D. Kälblein, H. Klauk, M. Halik, *Adv. Mater.* 2009, **21**, 3099.

Journal of Materials Chemistry C Accepted Manuscript

24. N. Straue, M. Rauscher, S. Walther, H. Faber, A. Roosen, *J. Mater. Sci.* 2009, **44**, 6011.

25. J. C. C. Fan, J. B. Goodenough, *J. Appl. Phys.* 1997, **48**, 3524.

26. T. Ishida, H. Kobayashi, Y. Nakato, *J. Appl. Phys.* 1993, **73**, 4344.

27. S. Jeong, Y.-G. Ha, J. Moon, A. Facchetti, T. J. Marks, *Adv. Mater.* 2010, **22**, 1346.

28. C. F. Baes and R. E. Mesmer, *The Hydrolysis of Cations*, Wiley, New York, 1976

29. C. J. Brinker, G. W. Scherer, *Sol-Gel Science*, Academic Press, San Diego, 1990.

30. Y. J. Kim, B. S. Yang, S. Oh, S. J. Han, H. W. Lee, J. Heo, J. K. Jeong, H. J. Kim, *ACS Appl. Mater. Interfaces* 2013, **5**, 3255.

Journal of Materials Chemistry C Accepted Manuscript